Reactive and Functional Polymers 201 (2024) 105949

Contents lists available at ScienceDirect

Reactive and Functional Polymers

journal homepage: www.elsevier.com/locate/react

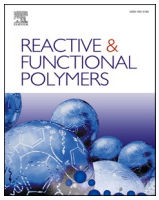

# Cyanate ester and polyethylene glycol based high temperature resistant shape memory polymer development for space applications

Sandaruwan Jayalath [a,b,c], Madhubhashitha Herath [a,d], Jayantha Epaarachchi [a,b,*], Eduardo Trifoni [e], Eleftherios E. Gdoutos [f,g], Bandu Samarasekara [h]

[a] Centre for Future Materials & Institute of Advanced Engineering and Space Sciences, University of Southern Queensland, Toowoomba, Australia
[b] School of Engineering, Faculty of Health, Engineering and Sciences, University of Southern Queensland, Toowoomba, Australia
[c] Division of Polymer and Chemical Engineering Technology, Institute of Technology University of Moratuwa, Diyagama, Homagama, Sri Lanka
[d] Department of Engineering Technology, Faculty of Technological Studies, Uva Wellassa University, Badulla, Sri Lanka
[e] Research School of Astronomy and Astrophysics, Australian National University, Canberra, Australia
[f] Graduate Aerospace Laboratories' California Institute of Technology, Pasadena, California, 91125, USA
[g] Proteus Space, Inc., Los Angeles, CA 90021, USA
[h] Deprartment of Materials Science and Engineering, University of Moratuwa, Sri Lanka

ARTICLE INFO

*Keywords:*
Shape memory polymers
High-temperature applications
Cyanate ester
Load-bearing applications

ABSTRACT

Cyanate Ester (CE)/Polyethylene glycol (PEG) based shape memory polymers (SMPs) offer a sustainable solution for space applications due to their high glass transition temperature and durability. PEG is a type of oligomer used as a shape memory effect modifier for CE. Due to the low toughness of CE-based polymers, they are often modified with epoxies to increase their toughness. However, the high molecular chain length of PEGs can also act as a plasticiser increasing the toughness of the CE/PEG-based SMPs instead of epoxies. This study explores the synergistic use of PEG with CE to optimise SMPs with comparable mechanical and shape memory properties, along with tailorable glass transition temperatures. During the synthesis, PEG 600, 1000, 2000 & 4000 were individually combined with CE monomers in varying stoichiometric ratios to produce a set of SMP specimens. Thermo-mechanical properties, and shape memory properties were experimentally obtained and graded as a function of different molecular weights of PEGs and their stoichiometric ratios. CE SMPs modified with PEG600 and 1000 exhibited stable storage moduli and therefore selected for further investigation. A single-parameter empirical model was developed to correlate $T_g$ with stoichiometric ratios, enabling the prediction of $T_g$ values for different CE: PEG600/1000 ratios or vice versa. The tensile and flexural properties at elevated temperatures were also studied. Notably, the use of lower molecular weight PEGs mitigated the storage modulus drops, while higher molecular weight PEGs significantly improved the toughness. Moreover, synthesised SMPs in the $T_g$ range of 125–130 °C using PEG600 and PEG1000 showed improved stability of storage modulus. The SMP with PEG600 showed better thermo-mechanical properties, storage modulus stability at higher temperatures, and shape memory behaviour compared to the SMP with PEG1000. This research contributes to developing robust and adaptable SMPs for space environments, bridging the gap between mechanical performance and shape memory capabilities.

## 1. Introduction

Shape memory polymers (SMPs) are a type of polymers that can be programmed and recovered under a specific stimulus such as heat, electricity, light, magnetism, pH levels, etc. [1–6]. Researchers all over the world are currently developing SMPs and SMP composites (SMPCs) to be used in space applications such as low earth orbit (LEO) satellites [7–11]. The majority of SMP components in space applications are comprised of Deployable hinges [9,12,13], booms [14], structures [15], solar arrays [16,17] and switches [18] which are not designed for load-bearing structural applications [19,20]. The main reason for using them only for non-structural applications is the inherently weaker thermo-

* Corresponding author at: School of Engineering, Faculty of Health, Engineering and Sciences, University of Southern Queensland, Toowoomba 4350, QLD, Australia.
*E-mail address:* Jayantha.Epaarachchi@unisq.edu.au (J. Epaarachchi).

https://doi.org/10.1016/j.reactfunctpolym.2024.105949
Received 29 February 2024; Received in revised form 26 May 2024; Accepted 28 May 2024
Available online 29 May 2024

**Table 1**
SMP synthesis, stoichiometric ratios.

| SMP Name | PEG ($M_n$) | BACE: PEG |
|---|---|---|
| A4 | 4000 | 21:1 |
| A2 | 2000 | 21:1 |
| A1 | 1000 | 21:1 |
| A0.6 | 600 | 21:1 |
| B4–1 | 4000 | 36:1 |
| B4–2 | 4000 | 26:1 |
| B4–3 | 4000 | 16:1 |
| B2–1 | 2000 | 16:1 |
| B2–2 | 2000 | 11:1 |
| B1–1 | 1000 | 16:1 |
| B1–2 | 1000 | 11:1 |
| B1–2 | 1000 | 6:1 |
| B0.6–1 | 600 | 11:1 |
| B0.6-2L | 600 | 6:1 |
| B0.6-2M | 600 | 7:1 |
| B0.6-2H | 600 | 8:1 |
| B1F | 1000 | 9.5:1 |
| B0.6F | 600 | 7.25:1 |
| B0.6–9 | 600 | 9:1 |

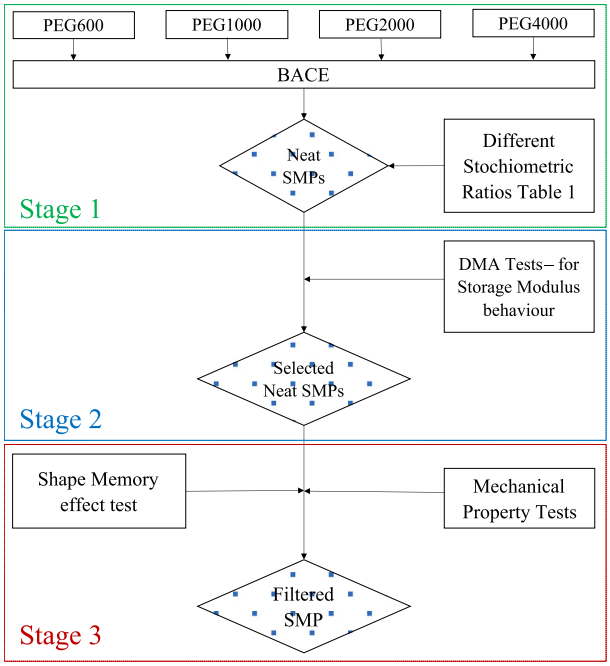


**Fig. 1.** Flowchart of the approach to filter a suitable SMP.

mechanical properties of the polymers [21]. As a rule of thumb, the temperature in environments such as LEO varies between −120 to +120 °C [22,23] and the lunar environment varies between −173 to +127 °C [24,25]. However, SMP components operating at LEO, medium earth orbit (MEO) and deep space environments can survive due to the zero gravity environment [26].

Notably, existing SMPs including the high-temperature SMPs in the last few decades were not designed to withstand the elevated temperature applications despite their higher $T_g$/ transition temperatures [26,27]. The activation temperature of the shape memory effect depends on the tan(δ) peak temperature or the storage modulus onset temperature. Since the tensile behaviour of the polymer can be predicted using the storage modulus of the polymer [28], the convenient activation temperature for load-bearing SMPs can be identified as the storage modulus onset temperature. Therefore, SMPs should exhibit an activation or transition temperature well above the operational range of the load-bearing component or structure, while maintaining consistent storage modulus behaviour.

To be qualified as a space-rated material, the material should undergo rigorous durability testing [26]. Cyanate ester-based SMPs are an emerging type of material that can overcome the limits set by several space durability test standards (ASTM E595 for the tests in vacuum, E2089 for the Atomic Oxygen Exposure and E512 for the electromagnetic and particulate radiation) and survive [29–32]. Cyanate ester has been often modified with epoxies [33] to increase their toughness as well as with nitriles and oligomers [34] to achieve the shape memory effect. Among them, cyanate esters modified with polyethylene glycols have shown outstanding durability in space-simulated environments [29–32]. However, continuously decreasing storage modulus with the temperature has been identified as a critical challenge for structural or load-bearing smart applications [26]. To address this, our research focuses on synthesising a novel cyanate ester SMP by leveraging different molecular weights of PEGs.

This project aims to synthesise and develop an SMP that is mechanically stable at high temperatures and capable of use in structural or load-bearing applications in space environments. Two major targets of this work are (1) to synthesise the SMP with a stable storage modulus till it glass transition temperature ($T_g$) and (2) to synthesise the SMP by varying the stoichiometric ratios to tune the $T_g$ in the range of 125–130 °C.

The outcome of this research will fill a gap in the space industry not only by providing a smart material that is suitable for LEO application but also a $T_g$ tailorable smart materials that can be used load load-bearing applications that can be used in spaces as well as terrestrial applications. Furthermore, the SMP can be further developed by adding reinforcing fibres becoming a shape memory polymer composite (SMPC). This research will further contribute significantly to the advancement of smart materials, ensuring their resilience in space environments while enabling adaptability for various applications.

## 2. Experimentation

### 2.1. Materials and specimen preparation

Bisphenol-A cyanate ester monomer (BACE, $M_n$ = 278.31) was purchased from Wenzhou Blue Dolphin New Material Co. Ltd., China and Polyethylene Glycols (PEG, $M_n$ = 600, 1000, 2000 and 4000) were purchased from Chem Supply Australia. SMPs were synthesised with different stochiometric ratios of BACE: PEG as indicated in Table 1. All the chemicals were used as received. BACE and PEG mixture was fully melted at 100 °C and mixed using a mechanical stirrer for 30 min. Then the mixture was degassed inside a vacuum oven at 100 °C. The bubble-free, transparent mixture was poured from a side of preheated Teflon peel ply-covered glass moulds. The curing cycle was 100 °C for 3 h, at 120 °C for 5 h, at 180 °C for 2 h and at 210 °C for 5 h. Finally, SMP sheets with 2 mm thickness were manufactured, and specimens were cut as per the ASTM/ISO standards using a waterjet cutter.

Fig. 1 shows the flowchart of the approach that has been used for this experiment. As the main parameters for the synthesis of the SMP, molecular weights of the shape memory property/ toughness modifiers (PEGs) and the stoichiometric ratio between BACE and PEGs were changed. Stage 1 shows the use of different PEG modifiers and stoichiometric ratio variations to understand their effect on the SMP behaviour. During Stage 2, each selected specimen's Tg vs BACE stoichiometric ratio graphs were fitted with a curve to get the generic model into an equation. This equation aimed to be modified and used to fabricate SMPs with tailored $T_g$ values that suit the environment. Stage 3 compares the selected SMP combinations in terms of mechanical and shape memory properties and chooses the SMP with adequate properties for space applications.

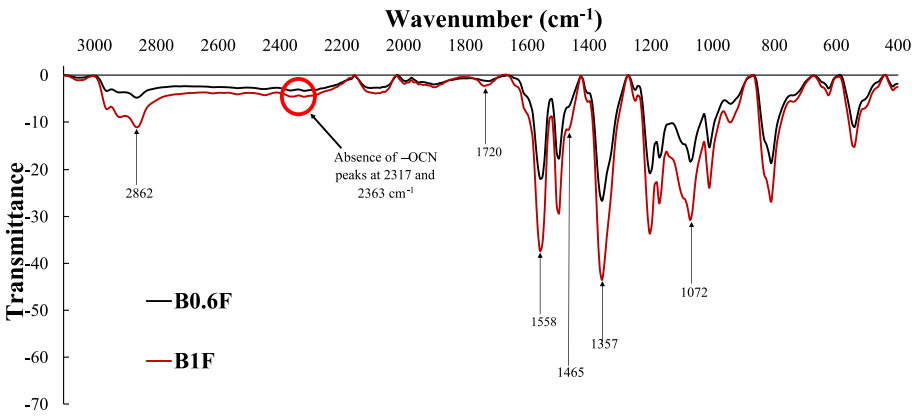


**Fig. 2.** FTIR spectral peaks of B0.6F and B1F SMPs.

### 2.2. Characterization

FTIR analysis of cured SMPs was carried out using SHIMADZU IRAffinnity-1S equipment to identify the chemical structure of the SMP. Dynamic mechanical analysis (DMA) of the SMPs was performed using TA Instruments hybrid rheometer (Discovery HR-2) under ASTM D7028 standard. Specimens from each SMP group were tested using the dual cantilever fixture with 1 Hz frequency, 25 μm axial displacement and temperature ramp of 5 °C/min from 25 to 200/250 °C. Each SMP sample was tested, and their storage modulus graphs were analysed as one of the main objectives of this experimental work. Storage modulus changes vs temperature were graphed in log scale and the storage onset value of the graph was taken as the primary $T_g$ value of the SMPs. Moreover, storage modulus stability was measured by calculating the secant storage modulus drop within the first 50% of the graph since it is the most linear part of each graph. During stage 2, differential scanning calorimeter (DSC) measurements were made on a TA instrument Discovery DSC-25 for cured and uncured samples of B1F and B0.6F. Samples were heated from 25 to 350 °C with a 10 °C/min heating rate. Thermograms of these cured and uncured graphs were utilised to calculate the curing percentage of the SMPs, and thermograms of the cured SMPs were used to calculate the secondary $T_g$ values of the SMPs.

All thermomechanical, mechanical and shape memory property tests were repeated three times (sample number, N) and the statistical parameters such as mean values (μ), standard deviations (s), and population standard uncertainties (u) were calculated using the measured values [35].

### 2.3. Shape memory effect evaluation

The fold-deploy test method was used to calculate shape fixity ($R_f$) and recovery ($R_r$) ratios using eqs. 1 and 2. During the $R_f$ evaluation [20], SMPs were kept at $T_g$ + 20 °C for 15 min and bent 90°/120°/180° with a diameter of 12 mm and the fixed angles were measured. After that, SMP were reheated, and the recovery process was monitored at the mentioned temperatures, and the $R_r$ was calculated. SMP $R_{r,110–150}$ were calculated by keeping the SMP strips at 110, 120, 130, 140 and 150 °C for 30 min inside the oven respectively. During this test, three measurements from three SMPs in each group were taken and their mean values and standard deviations were calculated for the analysis.

$$R_f = \frac{\theta_{fixed}}{\theta_{max}} \times 100\% \quad (1)$$

$$R_r = \frac{\theta_{fixed} - \theta_{end}}{\theta_{max}} \times 100\% \quad (2)$$

### 2.4. Mechanical property evaluation

SMPs' tensile strength, flexural strength and impact strength were determined according to ASTM D638, ASTM D790 and ASTM D6110 standards. An MTS 10 kN (Insight Electromechanical) uni-axial testing machine with an environmental chamber was used to evaluate the tensile behaviour and flexural strength at ambient and elevated temperatures at 110, 120, 130 and 140 °C. TYPE IV SMP specimens with 25 mm gauge length were used for the tensile test and tested with a 2 mm/min strain rate. 70 × 12.7 $mm^2$ rectangular specimens were used for the flexure test with the strain rate of 2 mm/min. An Instron Dynatup 8200 drop-weight impactor was used to conduct the impact test at the ambient temperature. Rectangular samples of 63.5 × 12.7 $mm^2$ with a 3 mm deep notch were used for the impact test.

## 3. Results and discussion

### 3.1. Synthesis reactions of the SMP

Understanding the chemical structure of the synthesised polymer is important to understand the behaviour of the SMP. FTIR analysis of the cured SMPs (Fig. 2) was used to identify peaks related to the chemical structure. Furthermore, previous work done by Kumar S. et al. (2014) [36] and Ma J.et al.(2014) [37] were used to develop (Fig. 3) the chemical reactions throughout the curing process. B0.6 and B1F samples were selected to analyse since they were synthesised to have the same $T_g$ values. According to the FTIR spectrum analysis of B0.6F and B1F SMPs, peaks from (O=C-N) transmittance groups of Isocyanurate appear at 1465 $cm^{-1}$ and 1720 $cm^{-1}$. Peaks at 1357 $cm^{-1}$ and 1558 $cm^{-1}$ appear due to the Triazine rings. The existence of the ether groups (-C-O-C-) and (-$CH_2$-) in PEGs can be confirmed by the peaks at 1072 $cm^{-1}$ and 2862 $cm^{-1}$ respectively. Furthermore, the absence of -OCN peaks at 2317 and 2363 $cm^{-1}$ shows that the SMPs have been fully cured.

### 3.2. Storage Modulus behaviour analysis

The storage modulus changes of samples A0.6, A1, A2 and A4 which have different molecular weights but the same 21:1 (BACE: PEG) ratio were compared (Fig. 4(a)). It is clear that the drop of storage modulus is significant with the increasing molecular weight/ molecular chain length of PEGs [38] hence showing the low stability of the SMPs with PEG2000 and PEG4000. For the SMP samples synthesised with PEG 600, 1000, 2000 and 4000, the mean secant gradients of the modulus drop (Fig. 4(b)) were 3.65, 8.74, 11.23 and 11.65 MPa/°C respectively and the $T_g$ (storage onset) value drop was from 232.96 ± 1.40, 222.66 ± 1.28, 188.47 ± 2.55 and 178.43 ± 2.87 °C respectively. As shown in the graphs in Fig. 4(a), SMPs synthesised with PEG600 and 1000 showed improved stability of the storage modulus with a modulus drop gradient

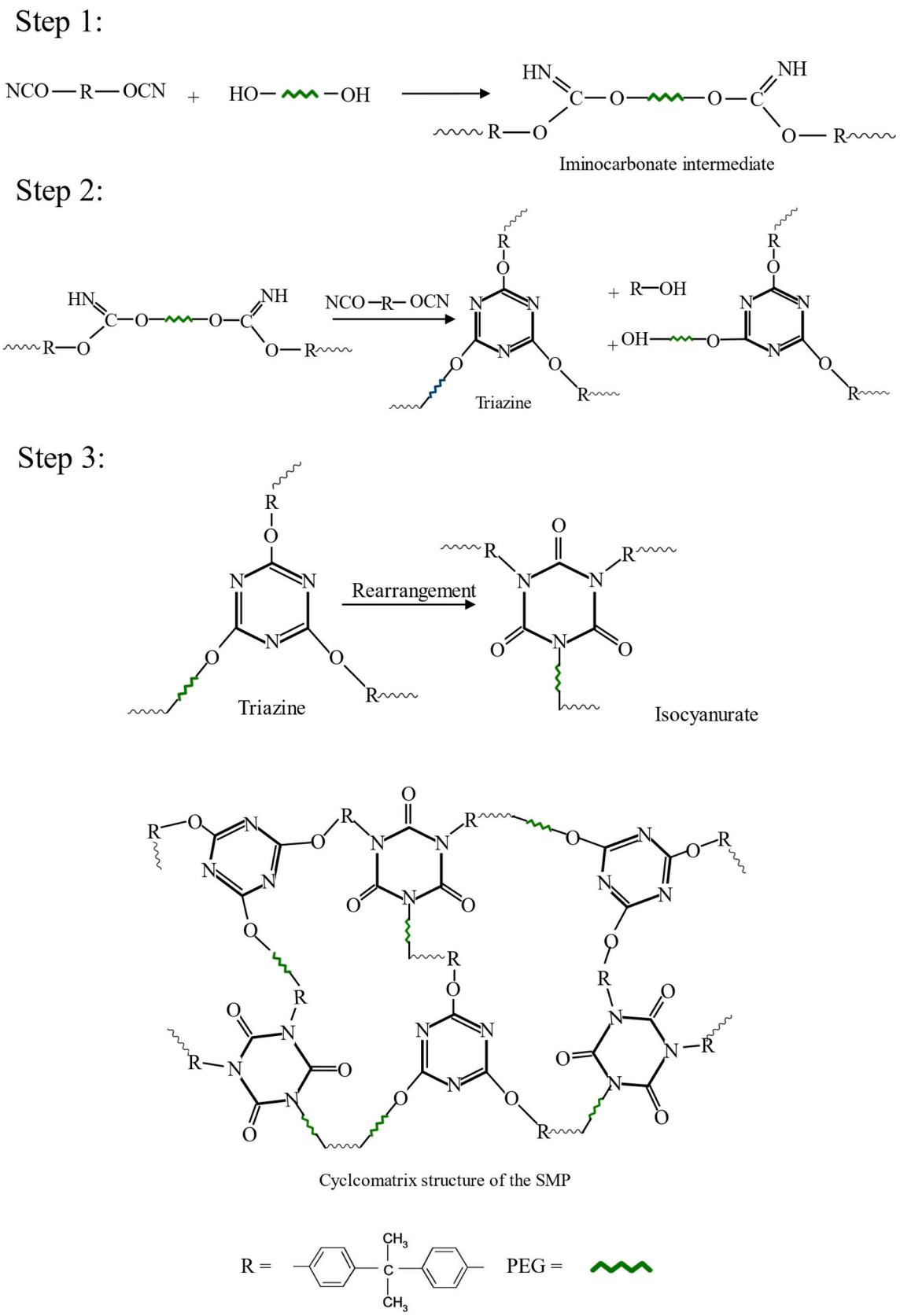


**Fig. 3.** Reactions of BACE and PEGs towards the SMP synthesis.

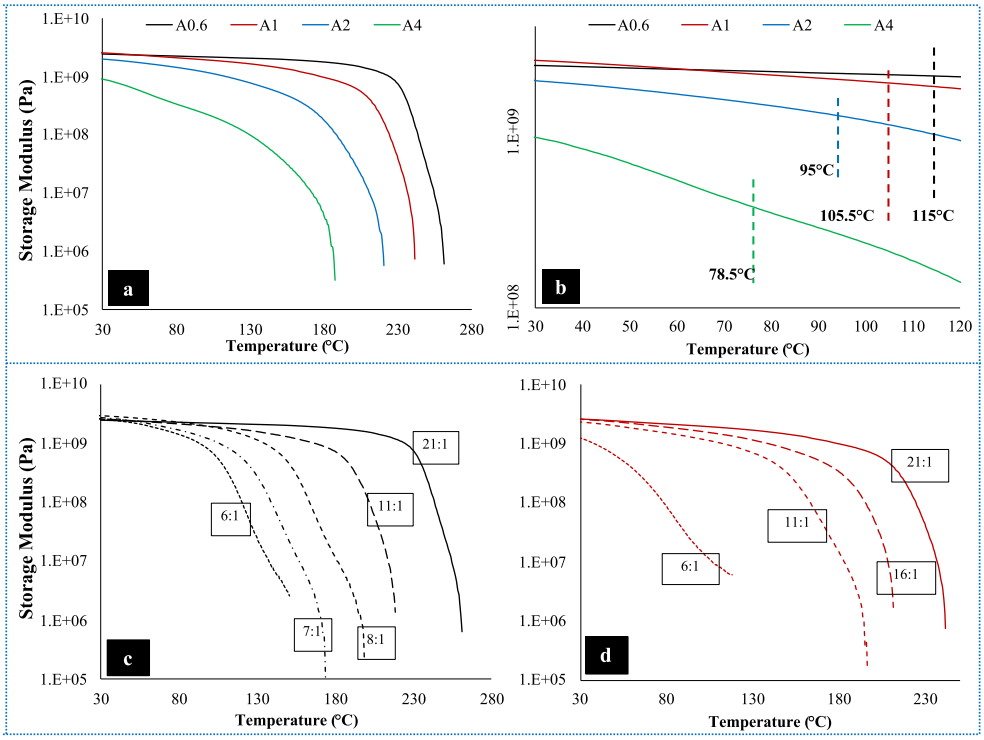


**Fig. 4.** (a) Storage Modulus changes with the different molecular weights of PEGs in the same stoichiometric ratio (21:1), (b) magnified section for the storage modulus drop secant gradient calculation. Storage modulus variation of the SMP with (c) PEG600 (B0.6 samples) and (d) PEG1000 (B1 samples) stoichiometric ratios.

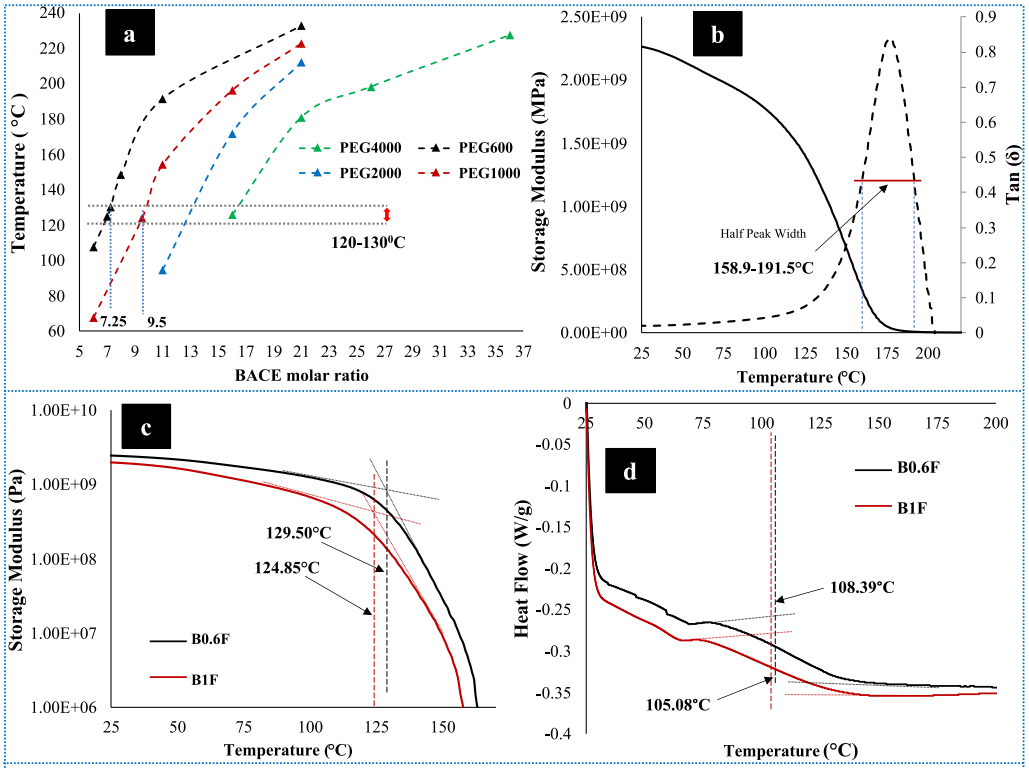


**Fig. 5.** (a)$T_g$ variation with the different molecular weights of PEGs and BACE: PEG stochiometric ratios. (b) Storage modulus and tan() graph of B0.6F-9 SMP. (c) DMA log storage modulus vs temperature and (d) DSC thermogram of the SMPs.

**Table 2**
Composition and thermomechanical properties of the SMP system.

| SMP Name | PEG Type | Stoichiometric Ratio (BACE:PEG) | Ave. $T_g$ (°C Log storage modulus onset) | $T_g$ (°C DSC) |
|---|---|---|---|---|
| B0.6F | 600 | 7.25:1 | 129.50 ± 0.33 | 108.39 ± 1.85 |
| B1F | 1000 | 9:1 | 124.85 ± 0.62 | 105.08 ± 0.74 |

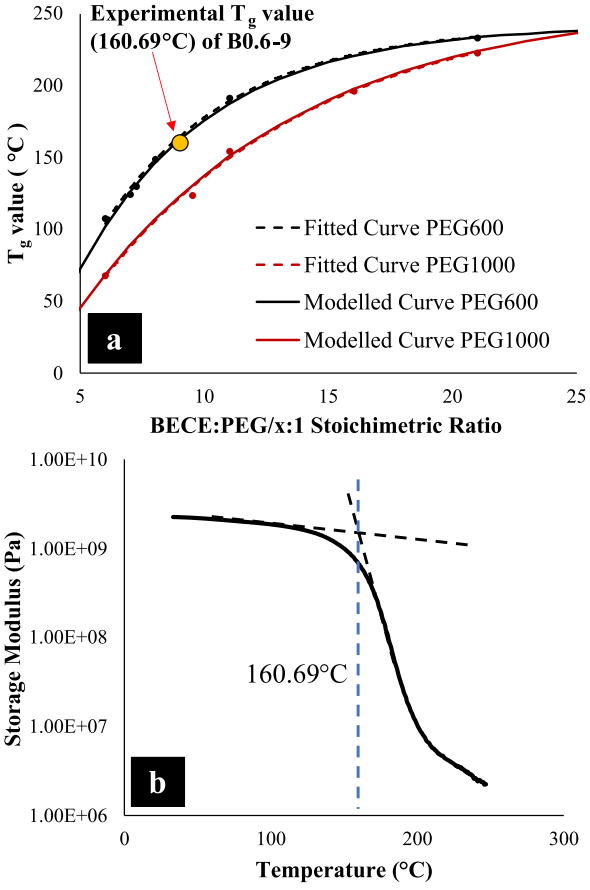


**Fig. 6.** (a) Fitted curves and modelled curves of the $T_g$ variation with respect to change of the stoichiometric ratios of BACE: PEG and (b) Storage modulus behaviour of B0.6–9 SMP with storage onset $T_g$ value of 160.69 ± 0.89 °C.

of less than 10 MPa/°C. Since this can be considered a stable storage modulus within a certain temperature range, SMPs with PEG600 and 1000 modifiers were selected for stage 3. Furthermore, storage modulus with the change of stochiometric ratios of the same molecular weights of PEGs (PEG600 and 1000) were also observed (Fig. 4(c & d)). It clearly shows that the amount of the PEG with the same molecular weight also influences the increased instability of the storage modulus hence decreasing the storage modulus onset $T_g$ of each SMP. The storage modulus drop gradient of the SMPs with B1 samples is quite significant compared to B0.6 samples due to the effects of both increasing moles and higher molecular chain length than B0.6. Apart from the shape memory effect, PEGs with long chain molecules have imparted some flexibility to the SMP and reduced its original $T_g$ value of the BACE by plasticising the parent matrix.

By changing the PEGs with different molecular weights and the stoichiometric ratios (Stage 1) between BACE: PEGs, the following conclusions were drawn.

**Table 3**
Fitted equations.

| Function type | Exponential decay function |
|---|---|
| Fitted Equations: Fitted curve PEG600 ($M_n = 600$) | |
| $T_g = 241.4 - 436.44e^{\left(\frac{-x}{0.0088M_n}\right)}$ | |
| $R^2$ value (Coefficient of Correlation) | 0.9964 |
| Fitted Equations: Fitted curve PEG1000 ($M_n = 1000$) | |
| $T_g = 258.31 - 376.62e^{\left(\frac{-x}{0.0088M_n}\right)}$ | |
| $R^2$ value (Coefficient of Correlation) | 0.9963 |
| Modelled Equation: for both curves: | |
| $T_g = (0.042M_n + 216.31) - (526.17 - 0.1496M_n)e^{\left(\frac{-x}{0.0088M_n}\right)}$ | |

$$T_g = (0.042M_n + 216.31) - (526.17 - 0.496M_n)e^{\left(\frac{-x}{0.0088M_n}\right)} \quad (3)$$

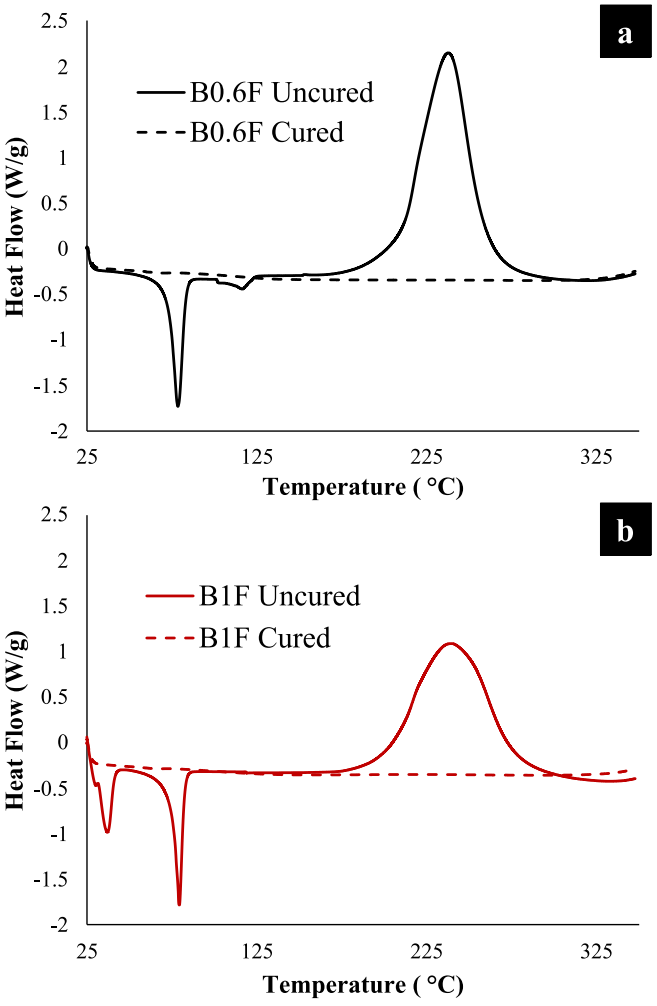


**Fig. 7.** Curing Kinetics of B0.6F (a) and B1F (b) SMPs.

**Table 4**
Shape fixity and recovery ratios of B0.6F and B1F SMP samples.

| Sample | No | Programmed angle | $R_f$ (%) at 25 °C | $R_r$(%) at $T_g$ + 20 °C |
|---|---|---|---|---|
| B0.6F | 1 | 90° | 100 ± 0.00 | 100 ± 00 |
| | 2 | 120° | 95.83 ± 0.71 | 100 ± 00 |
| | 3 | 180° | 92.22 ± 0.87 | 100 ± 00 |
| B1F | 1 | 90° | 100 ± 0.00 | 100 ± 00 |
| | 2 | 120° | 96.67 ± 0.99 | 100 ± 00 |
| | 3 | 180° | 97.78 ± 1.85 | 100 ± 00 |

1. The increase of the PEG molecular weights (from 600 to 4000) in the SMP reduces its storage modulus stability.
2. The increase of the certain PEG ratio in an SMP also reduces the storage modulus stability of the SMP.
3. SMPs made with 21:1 ratio using PEG600 and PEG1000 showed higher storage modulus stability with drop rates less than 10 MPa/°C.
4. The effect of using PEG with lower molecular weights than 600 can increase the storage modulus stability while decreasing the toughness of the SMP. In the same way, PEG with higher molecular weights than 4000 can lead to lower storage modulus stability and higher toughness in the SMP.
5. The reason for this behaviour was identified as the plasticisation of the BACE parent matrix from the long-chain molecules in PEGs.

### 3.3. Glass Transition Temperature Variation Analysis

The glass transition temperature can be often defined through many theoretical ways depending on the application such as recrystallisation, thermo-mechanical changes, modified cohesion energy method and other methods [39].To understand the $T_g$ variation with different molecular weights of PEGs and the stoichiometric ratios between BACE and PEGs, the log storage onset $T_g$ value of each sample mentioned in Table 1 were graphed (Fig. 5(a)) for their (BACE: PEG) stoichiometric ratios. B0.6F and B1F were synthesised using this behaviour in Fig. 5(a) to achieve the storage modulus onset $T_g$ in the range of 120–130 °C. $T_g$ values (Table 2) of the two SMPs were calculated considering the storage modulus onset point as well as the midpoint half-height values of the DSC curve as shown in Fig. 5(d). The log scale storage modulus onset point was selected as the primary $T_g$ value (Fig. 5(c)) since the authors of this research are looking to develop an SMP that can sustain stable mechanical properties at elevated temperatures closer to the $T_g$ value. Furthermore, the tan(δ) peak width at half of the peak height ($S_{1/2}$) of the B0.6F-9 samples shows the relaxation behaviour of the SMP in a range of 32.6 °C (Fig. 5(b)) compared to the 48 °C range in neat BACE [40]. The area under this peak has also been reduced from 7.1 (in neat BACE) to 3.45. The addition of PEG has caused a decrease in the width

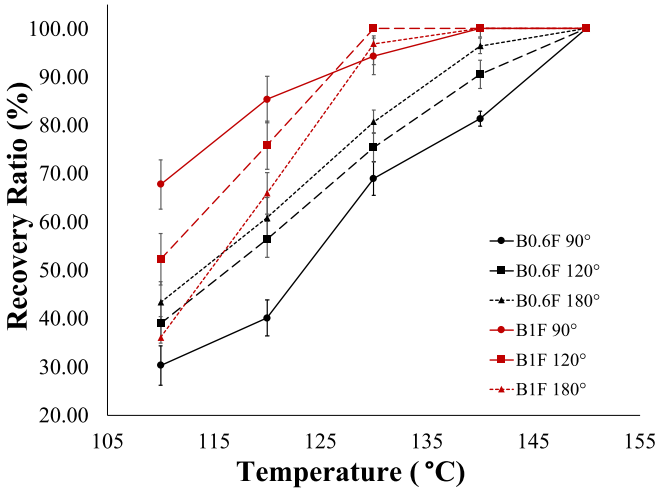


**Fig. 9.** Shape Recovery ratio variation of B0.6F and B1F.

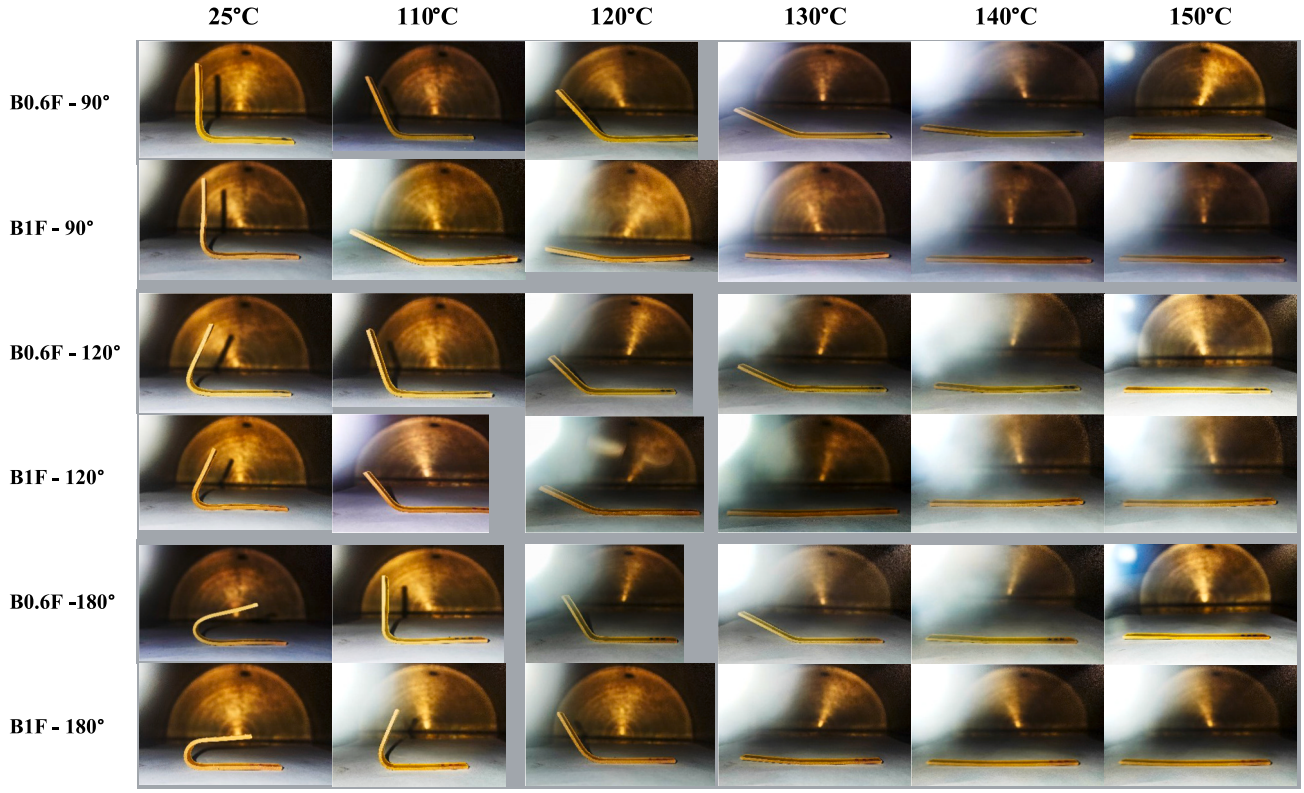


**Fig. 8.** Visual observation of B0.6F and B1F SMP shape recovery at 25, 110, 120, 130, 140 and 150 °C.

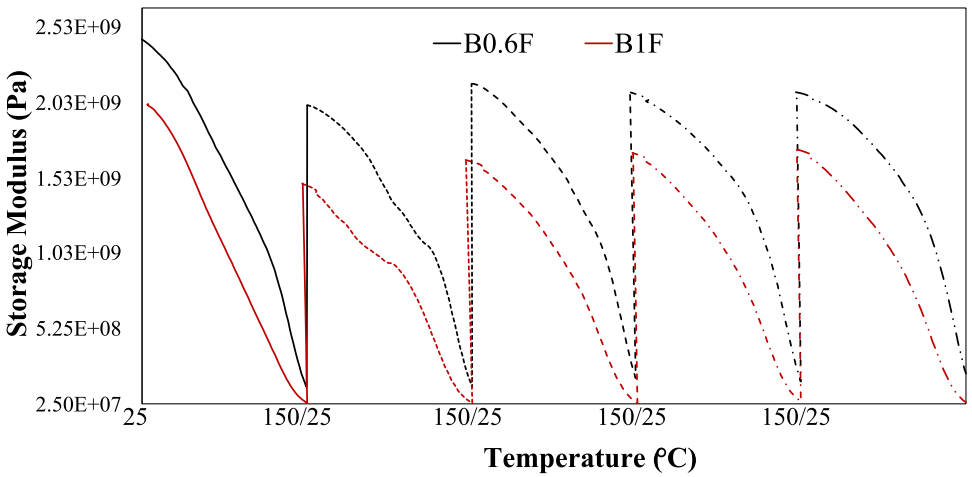


**Fig. 10.** Storage modulus variation of B0.6F and B1F over 5 thermal cycles.

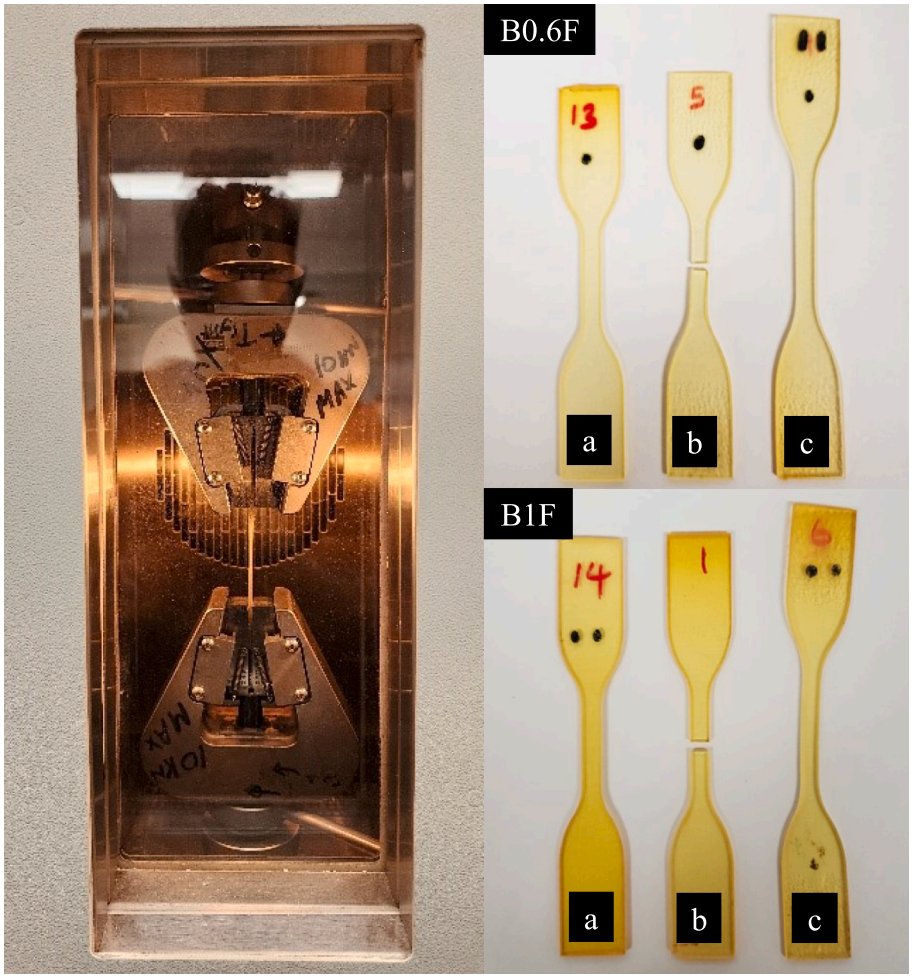


**Fig. 11.** Elevated temperature tensile testing setup and (a) tensile specimens, (b) tensile failure at room temperature and (c) elongated specimen at 140 °C.

and area of the tan(δ) peak indicating a higher mean of the network density and a greater homogeneity of the SMP network structure respectively.

After analysing the $T_g$ variation of B0.6F and B1F with respect to the change of stochiometric ratios change of the BACE, the data points were fitted into two curves as shown in Fig. 6(a) and equations (Table 3) were developed using the curve fitting technique. One model equation was derived by combining these two fitted empirical equations (Eq.3) where $T_g$ for specific BACE: PEG ratio or vice versa can be calculated by providing the molecular weight ($M_n$) of the PEG as 600 or 1000. To validate the developed model, an SMP was synthesised with BACE: PEG, 9:1 ratio and the SMP was tested with DMA and the storage modulus graph was analysed. According to the calculation using the model (Eq.3), the $T_g$ value was calculated as 162.13 °C. The experimental value

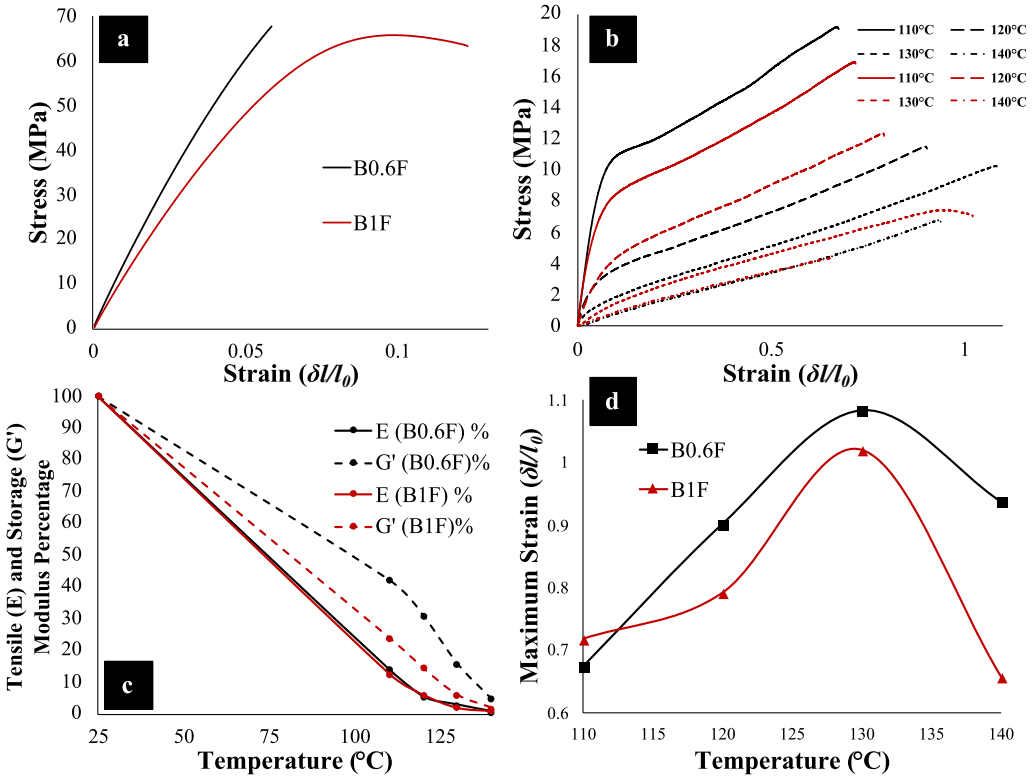


**Fig. 12.** (a) Tensile Stress vs Strain behaviour of B0.6F and B1F SMPs at room temperature (25 °C), (b) Stress vs Strain variations of B0.6F and B1F SMPs at increasing temperatures, (c) Tensile and Storage modulus percentage variation of B0.6F and B1F with the increasing temperature and (d) Max-strain behaviour of B0.6F and B1F with increasing temperature.

has given a close storage onset $T_g$ value at 160.69 ± 0.89 °C (Fig. 6(b)).

### 3.4. Curing kinetics verification of the selected SMPs

The chemical formulation and the curing kinetic parameters significantly affect the SMP properties. In this study, the authors aimed to compare the thermo-mechanical and shape memory properties against two different BACE: PEG combinations; hence curing parameters were kept constant. Fig. 7 illustrates the immediate DSC results of the uncured and cured SMP samples. It clearly showed the melting temperature of BACE monomer (in white crystal form) at 78.19–79.01 °C with an endothermic peak and the melting temperature of PEG1000 at ~36.64 °C. Furthermore, both uncured BACE: PEG resin mixtures have undergone an exothermic peak at 237.7 ± 0.78 °C and 239.8 ± 0.83 °C in B0.6F and B1F respectively. Similarly, cured Cyanate Ester SMP samples showed a quasi-linear response. The area under exothermic peaks represents the generated heat during the curing process. Exothermic peak area differences between uncured and cured B0.6F and B1F were 45.28 ± 1.12 and 17.36 ± 1.85 (W/g).°C respectively. Eq.4 determined the curing percentage cure percentage of the SMP was equal to 99.76% and 99.7% in B0.6F and B1F respectively, which provides a solid platform which to compare thermo-mechanical and shape memory properties.

$$\%Cure = \frac{|\Delta H_{uncured} - \Delta H_{cured}|}{|\Delta H_{uncured}|} * 100\% \quad (4)$$

### 3.5. Shape memory effect analysis

The shape memory effect of B0.6F and B1F were calculated and plotted as shown in Table 4 and Fig. 9. Furthermore, Fig. 8 shows the variations during the shape recovery of the SMPs with 90°, 120°, and 180° programmed angles and recovery percentages at 110, 120, 130, 140 and 150 °C temperatures. B1F showed 5.56% better shape fixity ratios compared to B0.6F during the programming of 180° angles. However, both have performed equally during the shape programming of lower angles having slight shape fixity ratios deviation from 0 to 0.84%.

As one of the important aims of this research, a lower recovery ratio of the SMPs was expected to happen below the $T_g$ and a higher recovery ratio, closer to the $T_g$. According to Fig. 8 and Fig. 9, B0.6F has shown lower recovery ratios in the satisfactory range of 70–80% while B1F is showing a premature recovery ratio of 90–100% at 130 °C. Hence, it is clear that B0.6F SMP has shown the required shape recovery behaviour compared to B1F SMP.

As a newly developed method, SMP samples were tested for their thermo-mechanical properties with DMA with 5 continuous thermal cycles, storage modulus variations over these 5 thermal cycles were graphed with both B0.6F and B1F samples (Fig. 10). All the thermal cycles were programmed from 25 to150°C. After the first cycle, storage modulus in both B0.6F and B1F decreased from 18.1% and 26.1% respectively. B0.6F kept the storage modulus between 2 and 2.15 GPa in the next 4 cycles while B1F kept its storage modulus gradually increasing from 1.49 to 1.71 GPa in the next 4 cycles. This can be explained through the chain scission of the PEGs that happens during the thermomechanical cycles [26]. Since PEG crosslinks (soft segments that are responsible for the shape recovery effect) are subjected to break before more thermally stable isocyanurate and triazine network structures, it can affect the SMP by increasing the shape fixity while decreasing the shape recovery properties. However, this behaviour can be considered a stable thermomechanical behaviour in both SMPs since there is no significant drop in the maximum storage modulus behaviour after the first thermo-mechanical cycle.

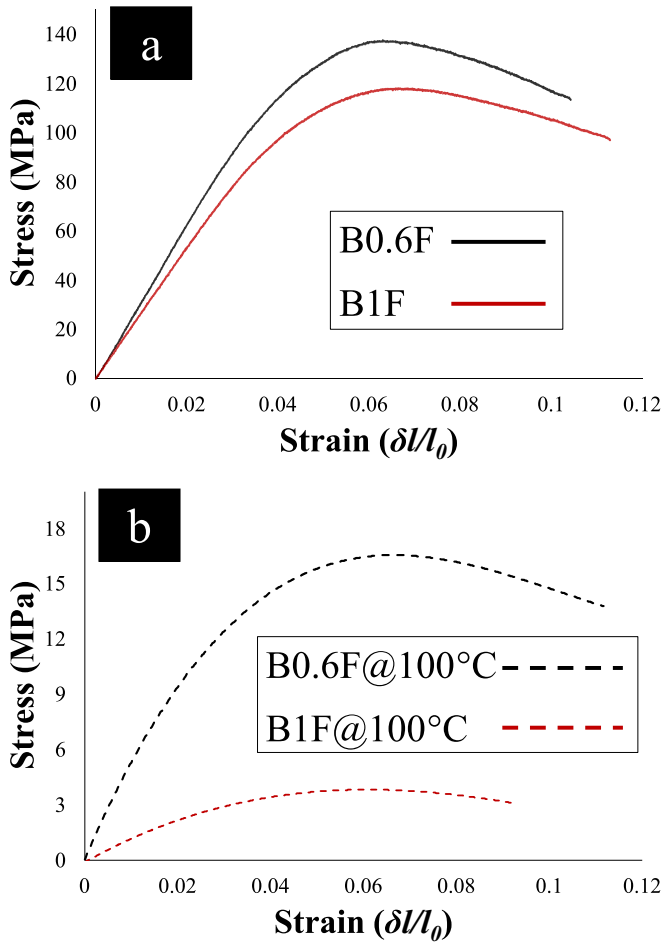


**Fig. 13.** Flexural Stress vs Strain behaviour of the SMPs (a) at room temperature and (b) at 110 °C.

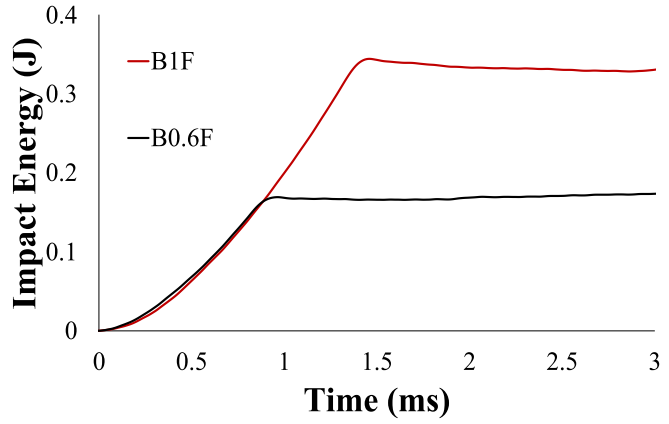


**Fig. 14.** Impact Energy absorbance of B0.6F and B1F specimens.

### 3.6. Mechanical property analysis

Both B0.6F and B1F were synthesised to have the same $T_g$ range (125–130 °C). Therefore, the mechanical properties of the SMPs are expected to show the same shape memory behaviour that can be activated in the same temperature range. The elevated temperature testing setup and the tensile behaviour of the SMPs are shown in Fig. 11. The tensile behaviour of the two SMPs (B0.6F and B1F) at room temperature (25 °C) and elevated temperatures is shown in Fig. 12(a & b) respectively. B0.6F showed a higher tensile modulus of 1.15 ± 0.12 GPa and lower max-strain of 0.059 ± 0.004 and B1F showed a lower tensile modulus of 0.897 ± 0.010 GPa and comparatively higher max-strain of 0.123 ± 0.008. Both samples showed a maximum stress in the range of 65.94–67.64 MPa. However, the mechanical properties of these two samples with the increasing temperatures (Fig. 12) showed a significant drop in the tensile modulus and yield strength of the two SMPs while increasing the strain. B1F showed a drop of 87.29% and 74.4%, and B0.6F showed a drop of 86.09% and 71.8% from their original tensile modulus and stress at break respectively.

Furthermore, the change of tensile modulus (E) was graphed with respect to their storage modulus (G′) as shown in Fig. 12(c). It shows a gradual drop of both tensile and storage modulus values with the increasing temperature. Even though the storage modulus of B0.6F is slightly higher than B1F, the tensile modulus of both SMPs shows similar tensile modulus drop with increasing temperature. The weak thermal stability of PEGs can be mentioned as a reason for this behaviour. It is interesting to note that the yield stress and yield strain were decreased with increasing temperature showing no yield point after the $T_g$. This is caused by separated crosslinks from the polymer chains with the increased temperature causing lower intermolecular bonding and molecular rigidity [41].

The max-strain behaviour of the SMPs with the temperature showed an increase of the strain and a sudden drop after passing 130 °C as shown in Fig. 12(d). It is worth noticing that the max strain is recorded inside the $T_g$ range (125–130 °C), and strain drop afterwards can be due to the weakening thermal stability of PEGs. This max-strain behaviour under increasing temperature graph also shows 6.33% less max strain and low strain trend in B1F (PEG1000) compared to the B0.6F. This behaviour aligns with the storage modulus drop of the SMPs with the increasing temperature which is influenced by the molecular weight/chain length of the PEGs.

The flexural behaviour of the SMPs is shown in Fig. 13 at room temperature and 100 °C. It shows an 87.96% flexural stress drop in B0.6F and a 96.6% drop in B1F. While this data shows lower flexural strength in B1F SMP, it also indicates that B1F SMPs are easier to program into different shapes at lower temperatures than B0.6F SMP. This is due to the higher molecular weight/ chain length of the PEG1000 and its weak thermal stability at higher temperatures. However, pointing out the effect of the molecular weight difference in each SMP, the impact energy absorbance (Fig. 14) is 50.87% higher in B1F than in B0.6F.

### 3.7. Selection of materials and ratios for the final SMP composition

The gathered information through the various experiments is depicted in Fig. 15. According to that, it is important to note that the selected two SMPs (B0.6F and B1F) show significantly improved thermo-mechanical properties. The material B1F showed relatively better performances in shape fixity, impact energy absorbance, and ductility. However, B0.6F has shown better mechanical properties such as tensile strength, tensile modulus, flexural strength and relatively higher storage modulus and tensile properties at elevated temperatures. Therefore, B0.6F SMP shows the potential for shape memory components due to the following three major reasons. (1) comparable stability of the storage modulus with increasing temperature (Fig. 4(c & d)), (2) higher shape retention ability till the targeted temperature during shape recovery (Fig. 9), and (3) higher and constant storage modulus during 5 thermomechanical cycles (Fig. 10). Furthermore, the properties of existing SMPs which were developed for high temperature applications were also compared. Table 5 shows that B0.6F SMP shows comparatively equal properties in terms of mechanical and shape memory properties.

## 4. Conclusion

This paper details the synthesisation of an SMP with optimized thermomechanical and shape memory properties and the potential to be

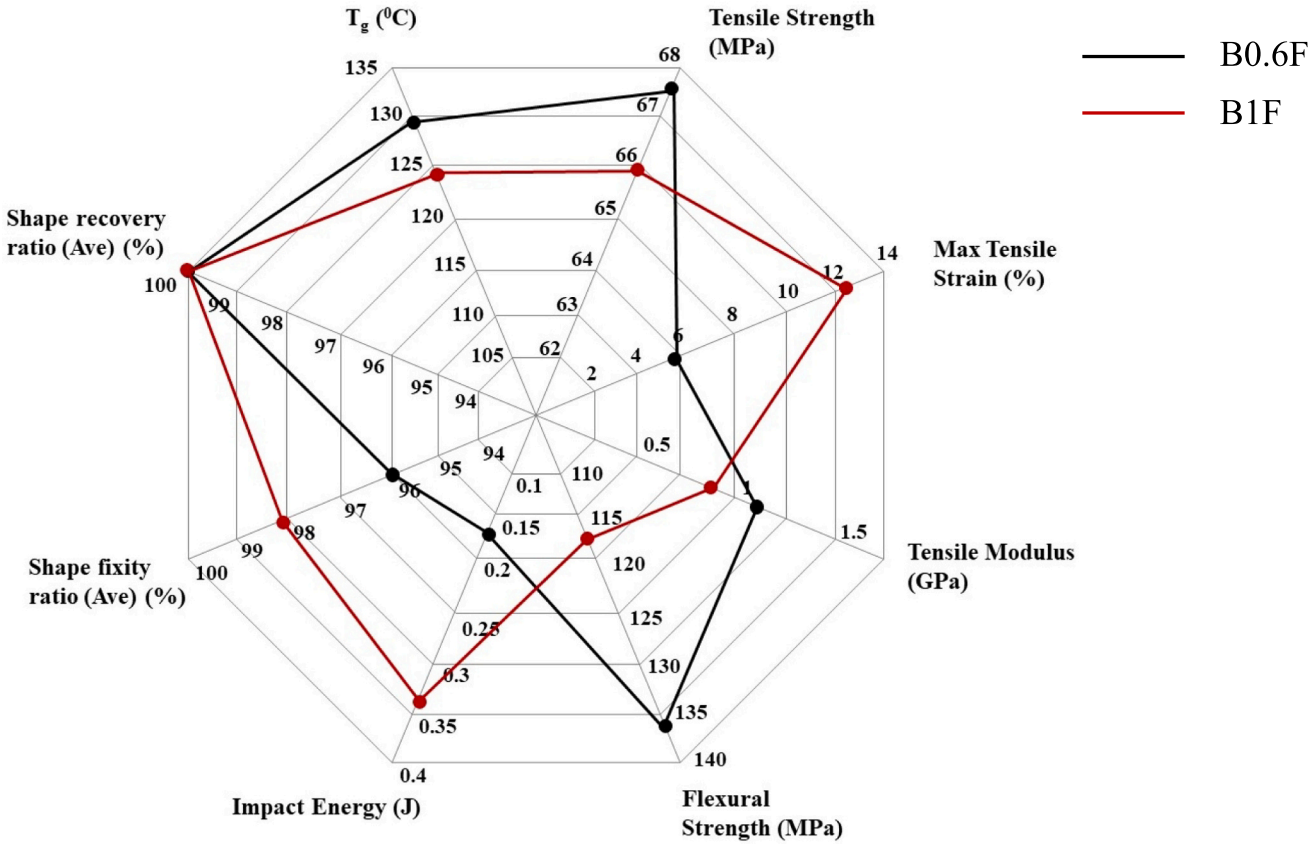


**Fig. 15.** Property comparison diagram of B0.6F and B1F SMPs.

**Table 5**
Comparison of properties of existing SMPs.

| Based polymer | Tensile Strength (MPa) | Tensile Strain (%) | Tensile Modulus (GPa) | Shape Fixity (%) | Shape Recovery (%) | Reference |
|---|---|---|---|---|---|---|
| B0.6F | 67.64 | 5.9 | 1.15 | 96.02 | 100 | – |
| B1F | 65.94 | 12.3 | 0.89 | 98.15 | 100 | – |
| BACE | – | – | – | 98.00 | 100 | 2014 [36] |
| BACE | 70.60 | 4.5 | 2.71 | 98.20 | 95 | 2022 [42] |
| BACE | 66.00 | 7.0 | 1.90 | 97.60 | 97.6 | 2023 [30] |
| MPA (poly-N, N′-(*m*-phenylene) isophthalamide) | ~70.00 | 15.0 | ~1.90 | 99.00 | 97 | 2024 [43] |

used for applications at temperatures higher than room temperature. Cyanate ester resin was mixed with different molecular weights of PEGs until the most stable thermo-mechanical properties of the mixture (SMP) were achieved. The thermomechanical behaviour of 16 different compositions were experimentally analysed to identify the most stable thermo-mechanically SMP configuration. During the process of synthesisation, it has been noticed that the increased molecular weight of PEG significantly de-stabilize the thermo-mechanical behaviour. The reason for this behaviour was identified as the plasticisation of the BACE parent matrix from the long-chain molecules in PEGs.

Two key SMP configurations were selected B0.6F and B1F and continued the experimental programme to identify the best SMP configuration. An empirical model was developed to calculate the required chemical stoichiometric ratios to synthesise SMPs based on PEG600 and PEG1000 to achieve the required $T_g$ values. The model predictions have shown an excellent correlation with the experimentally obtained $T_g$ values for various CE: PEG molar ratios.

B0.6F and B1F SMPs were tested for shape memory properties and mechanical properties at a wider range of temperatures from 30C to 140C. The following are the major conclusions drawn from this research.

1. Both B0.6F and B1F SMPs show 100% shape recovery. However, the shape retention ability of B0.6F with increasing temperature plays are major role during the application level, making the B0.6F SMP superior compared to B1F.
2. B0.6F tends to show better storage modulus stability with increasing temperature as well as over 5 thermomechanical cycles during the dynamic mechanical analysis (DMA).
3. B0.6F shows higher tensile and flexural properties than B1F at room temperature 30 °C as well as at high temperatures from 100 to 140 °C.
4. B1F shows higher impact energy (toughness) and tensile strain than B0.6F due to higher molecular chain length in PEG1000 crosslinks.

In summary, this research has successfully developed a novel SMP suitable for the manufacturing of load-bearing components and structures for LEO and lunar environments. The outcomes of this research which is a robust material for structural applications beyond room temperature, contribute a wealth of new knowledge to the space industry. Further, the incorporation of a range of reinforcing fibres could transform these SMPs into SMP composites for a broader range of space

applications.

## CRediT authorship contribution statement

**Sandaruwan Jayalath:** Conceptualization, Data curation, Formal analysis, Investigation, Methodology, Resources, Software, Visualization, Validation, Writing – original draft. **Madhubhashitha Herath:** Conceptualization, Supervision, Writing – review & editing. **Jayantha Epaarachchi:** Conceptualization, Funding acquisition, Supervision, Writing – review & editing. **Eduardo Trifoni:** Supervision. **Eleftherios E. Gdoutos:** Supervision. **Bandu Samarasekara:** Supervision.

## Declaration of competing interest

The authors declare that they have no known competing financial interests or personal relationships that could have appeared to influence the work reported in this paper.

## Data availability

Data will be made available on request.

## Acknowledgement

The authors would like to extend their gratitude to Dr. Choman Salih (Research Facility Manager), Dr. Mazhar Peerzada (Senior Research Technical Officer), Mr. Oliver Kinder (Senior Technical Officer) and Mr. Nathan Strenzel (Technical Officer) at the University of Southern Queensland, for their valuable assistance in this research.

## References

[1] H. Lu, Z. Li, X. Qi, L. Xu, Z. Chi, D. Duan, M.Z. Islam, W. Wang, X. Jin, Y. Zhu, Y. Fu, L. Cui, Y. Zhuang, Y. Dong, Flexible, electrothermal-driven controllable carbon fiber/poly(ethylene-co-vinyl acetate) shape memory composites for electromagnetic shielding, Compos. Sci. Technol. 207 (2021) 108697, https://doi.org/10.1016/j.compscitech.2021.108697.

[2] T. Mu, L. Liu, X. Lan, Y. Liu, J. Leng, Shape memory polymers for composites, Compos. Sci. Technol. 160 (2018) 169–198, https://doi.org/10.1016/j.compscitech.2018.03.018.

[3] J. Leng, X. Lan, Y. Liu, S. Du, Shape-memory polymers and their composites: stimulus methods and applications, Prog. Mater. Sci. 56 (2011) 1077–1135, https://doi.org/10.1016/j.pmatsci.2011.03.001.

[4] W. Wang, Y. Liu, J. Leng, Recent developments in shape memory polymer nanocomposites: actuation methods and mechanisms, Coord. Chem. Rev. 320–321 (2016) 38–52, https://doi.org/10.1016/j.ccr.2016.03.007.

[5] M. Herath, J. Epaarachchi, M. Islam, L. Fang, J. Leng, Light activated shape memory polymers and composites: a review, Eur. Polym. J. 136 (2020) 109912, https://doi.org/10.1016/j.eurpolymj.2020.109912.

[6] Y. Wang, G. Zhu, X. Cui, T. Liu, Z. Liu, K. Wang, Electroactive shape memory effect of radiation cross-linked SBS/LLDPE composites filled with carbon black, Colloid Polym. Sci. 292 (2014) 2311–2317, https://doi.org/10.1007/s00396-014-3266-0.

[7] D. Margoy, I. Gouzman, E. Grossman, A. Bolker, N. Eliaz, R. Verker, Epoxy-based shape memory composite for space applications, Acta Astronaut. 178 (2021) 908–919, https://doi.org/10.1016/j.actaastro.2020.08.026.

[8] X. Lan, Y. Liu, H. Lv, X. Wang, J. Leng, S. Du, Fiber reinforced shape-memory polymer composite and its application in a deployable hinge, Smart Mater. Struct. 18 (2009), https://doi.org/10.1088/0964-1726/18/2/024002.

[9] R. Barrett, W. Francis, E. Abrahamson, M.S. Lake, M. Scherbarth, Qualification of elastic memory composite hinges for spaceflight applications, Collect. Tech. Pap. - AIAA/ASME/ASCE/AHS/ASC Struct. Struct. Dyn. Mater. Conf 8 (2006) 5379–5388, https://doi.org/10.2514/6.2006-2039.

[10] M.J. Jo, H. Choi, H. Jang, W.R. Yu, M. Park, Y. Kim, J.K. Park, J.H. Youk, Preparation of epoxy-based shape memory polymers for deployable space structures using diglycidyl ether of ethoxylated bisphenol-a, J. Polym. Res. 26 (2019), https://doi.org/10.1007/s10965-019-1801-x.

[11] Y. Liu, H. Du, L. Liu, J. Leng, Shape memory polymers and their composites in aerospace applications: a review, Smart Mater. Struct. 23 (2014), https://doi.org/10.1088/0964-1726/23/2/023001.

[12] T.D. Dao, N.S. Ha, N.S. Goo, Design , fabrication , and bending test of shape memory polymer composite hinges for space deployable structures, 2017, https://doi.org/10.1177/1045389X17742728.

[13] V.L. Le, V.T. Le, N.S. Goo, Deployment performance of shape memory polymer composite hinges at low temperature, J. Intell. Mater. Syst. Struct. 30 (2019) 2625–2638, https://doi.org/10.1177/1045389X19873403.

[14] J. Banik, S. Kiefer, M. Lapointe, P. Lacorte, On-orbit validation of the roll-out solar array, IEEE Aerosp. Conf. Proc. 2018 (2018-March) 1–9, https://doi.org/10.1109/AERO.2018.8396390.

[15] H.M.C.M. Herath, J.A. Epaarachchi, M.M. Islam, J. Leng, Carbon fibre reinforced shape memory polymer composites for deployable space habitats, Eng. J. Inst. Eng. Sri Lanka. 52 (2019) 1, https://doi.org/10.4038/engineer.v52i1.7323.

[16] X. Lan, L.W. Liu, F.H. Zhang, Z.X. Liu, L.L. Wang, Q.F. Li, F. Peng, S. Da Hao, W. X. Dai, X. Wan, Y. Tang, M. Wang, Y.Y. Hao, Y. Yang, C. Yang, Y.J. Liu, J.S. Leng, World's first spaceflight on-orbit demonstration of a flexible solar array system based on shape memory polymer composites, Sci. China Technol. Sci. 63 (2020) 1436–1451, https://doi.org/10.1007/s11431-020-1681-0.

[17] F. Li, L. Liu, X. Lan, C. Pan, Y. Liu, J. Leng, Q. Xie, Ground and geostationary orbital qualification of a sunlight-stimulated substrate based on shape memory polymer composite, Smart Mater. Struct. 28 (2019), https://doi.org/10.1088/1361-665X/ab18b7.

[18] C. Zeng, L. Liu, Y. Du, M. Yu, X. Xin, P. Xu, F. Li, L. Wang, F. Zhang, Y. Liu, J. Leng, Space-deployable device based on shape memory cyanate ester composites, Compos. Commun. 42 (2023) 101690, https://doi.org/10.1016/j.coco.2023.101690.

[19] K.D.C. Emmanuel, L.H.J. Jeewantha, H.M.C.M. Herath, J.A. Epaarachchi, T. Aravinthan, Shape memory polymer composite circular and square hollow members for deployable structures, Compos. Part A Appl. Sci. Manuf. 171 (2023) 107559, https://doi.org/10.1016/j.compositesa.2023.107559.

[20] K.D.C. Emmanuel, H.M.C.M. Herath, L.H.J. Jeewantha, J.A. Epaarachchi, T. Aravinthan, Thermomechanical and fire performance of DGEBA based shape memory polymer composites for constructions, Constr. Build. Mater. 303 (2021) 124442, https://doi.org/10.1016/j.conbuildmat.2021.124442.

[21] E. Plati, J.G. Williams, Effect of temperature on the impact fracture toughness of polymers, Polymer (Guildf). 16 (1975) 915–920, https://doi.org/10.1016/0032-3861(75)90213-X.

[22] R. Verker, A. Bolker, Y. Carmiel, I. Gouzman, E. Grossman, T.K. Minton, S. Remaury, Ground testing of an on-orbit atomic oxygen flux and ionizing radiation dose sensor based on material degradation by the space environment, Acta Astronaut. 173 (2020) 333–343, https://doi.org/10.1016/j.actaastro.2020.04.065.

[23] K.K.G. de Finckenor, M. Miria, Space Environmental Effects, 2009, pp. 521–527, https://doi.org/10.1201/9781420084320-c27.

[24] H. Benaroya, The Lunar Environment, in: Build, Springer International Publishing, Cham, Habitats Moon, 2018, pp. 42–84, https://doi.org/10.1007/978-3-319-68244-0_3.

[25] H.J. Fincannon, Lunar Environment and Lunar Power Needs (2020) 1–5.

[26] S. Jayalath, M. Herath, J. Epaarachchi, E. Trifoni, E.E. Gdoutos, L. Fang, Durability and long-term behaviour of shape memory polymers and composites for the space industry - a review of current status and future perspectives, Polym. Degrad. Stab. 211 (2023) 110297, https://doi.org/10.1016/j.polymdegradstab. 2023.110297.

[27] Z. Chi, C. Wang, Y. Dong, Y. Zhou, H. Xu, Z. Islam, C. Qian, Y. Fu, MXene/epoxy-based shape memory nanocomposites with highly stable thermal-mechanical coupling effect for constructing an effective information transmission medium, Compos. Sci. Technol. 225 (2022) 109505, https://doi.org/10.1016/j.compscitech.2022.109505.

[28] S. Cao, X. Wang, Z. Wu, Evaluation and prediction of temperature-dependent tensile strength of unidirectional carbon fiber-reinforced polymer composites, J. Reinf. Plast. Compos. 30 (2011) 799–807, https://doi.org/10.1177/0731684411411002.

[29] L. Wang, F. Zhang, Y. Liu, S. Du, J. Leng, Thermal, mechanical and shape fixity behaviors of shape memory cyanate under γ-ray radiation, Smart Mater. Struct. 31 (2022), https://doi.org/10.1088/1361-665X/ac5538.

[30] Z. Ping, F. Xie, X. Gong, L. Liu, J. Leng, Y. Liu, Effects of accelerated aging on thermal, mechanical and shape memory properties of cyanate-based shape memory polymer: III vacuum thermal cycling, Polymers (Basel). 15 (2023) 1893, https://doi.org/10.3390/polym15081893.

[31] F. Xie, L. Liu, X. Gong, L. Huang, J. Leng, Y. Liu, L. Liu, J. Leng, Y. Liu, X. Gong, L. Huang, J. Leng, Y. Liu, L. Liu, J. Leng, Y. Liu, X. Gong, L. Huang, J. Leng, Y. Liu, L. Liu, J. Leng, Y. Liu, X. Gong, L. Huang, J. Leng, Y. Liu, Effects of accelerated aging on thermal, mechanical, and shape memory properties of a cyanate-based shape memory polymer: II atomic oxygen, Polym. Degrad. Stab. 186 (2021) 109515, https://doi.org/10.1016/j.polymdegradstab. 2021.109515.

[32] F. Xie, L. Liu, X. Gong, L. Huang, J. Leng, Y. Liu, Effects of accelerated aging on thermal, mechanical and shape memory properties of cyanate-based shape memory polymer: I vacuum ultraviolet radiation, Polym. Degrad. Stab. 138 (2017) 91–97, https://doi.org/10.1016/j.polymdegradstab. 2017.03.001.

[33] A. Salunke, S. Sasidharan, J.C. Gopinathapanicker, B. Kandasubramanian, A. Anand, Cyanate ester epoxy blends for structural and functional composites, Ind. Eng. Chem. Res. 60 (2021) 3260–3277, https://doi.org/10.1021/acs.iecr.0c05008.

[34] H.T.S. Jayalath, M. Herath, J. Epaarachchi, Cyanate Esters as a High Performing Shape Memory Polymer: A Review, in: Mater. Today Proc, Elsevier Ltd, 2022, pp. 693–700, https://doi.org/10.1016/j.matpr.2022.02.121.

[35] V.R. Meyer, Measurement uncertainty, J. Chromatogr. A 1158 (2007) 15–24, https://doi.org/10.1016/j.chroma.2007.02.082.

[36] K.S. Santhosh Kumar, A.K. Khatwa, C.P. Reghunadhan Nair, High transition temperature shape memory polymers (SMPs) by telechelic oligomer approach, React. Funct. Polym. 78 (2014) 7–13, https://doi.org/10.1016/j.reactfunctpolym.2014.02.008.

[37] J. Ma, X. Lei, D. Tian, L. Yuan, C. Liao, Curing behavior and network formation of cyanate ester resin/polyethylene glycol, J. Appl. Polym. Sci. 132 (2015) 1–11, https://doi.org/10.1002/app.41841.

[38] X. Zeng, S. Yu, M. Lai, R. Sun, C.P. Wong, Tuning the mechanical properties of glass fiber-reinforced bismaleimide-triazine resin composites by constructing a flexible bridge at the interface, Sci. Technol. Adv. Mater. 14 (2013), https://doi.org/10.1088/1468-6996/14/6/065001.
[39] W.M. Groenewoud, Characterisation of Polymers by Thermal Analysis, Elsevier, 2001, https://doi.org/10.1016/B978-0-444-50604-7.X5000-6.
[40] U. Szeluga, P. Moryc, Viscoelastic properties and morphology of dicyanate ester/epoxy co-polymers modified with polysiloxane and butadiene–acrylonitrile rubbers, J. Therm. Anal. Calorim. 114 (2013) 137–146, https://doi.org/10.1007/s10973-012-2899-9.
[41] A.E. Mayr, W.D. Cook, G.H. Edward, Yielding behaviour in model epoxy thermosets - I. Effect of strain rate and composition, Polymer (Guildf). 39 (1998) 3719–3724, https://doi.org/10.1016/S0032-3861(97)10334-2.
[42] Z. Tang, J. Gong, P. Cao, L. Tao, X. Pei, T. Wang, Y. Zhang, Q. Wang, J. Zhang, 3D printing of a versatile applicability shape memory polymer with high strength and high transition temperature, Chem. Eng. J. 431 (2022) 134211, https://doi.org/10.1016/j.cej.2021.134211.
[43] B.C. Kholkhoev, K.N. Bardakova, A.N. Nikishina, Z.A. Matveev, Y.M. Efremov, A. A. Frolova, A.A. Akovantseva, E.N. Gorenskaia, N.A. Verlov, P.S. Timashev, V. F. Burdukovskii, 4D-printing of mechanically durable high-temperature shape memory polymer with good irradiation resistance, Appl. Mater. Today 36 (2024) 102022, https://doi.org/10.1016/j.apmt.2023.102022.